Switching-free time-domain optical quantum computation with quantum teleportation

Warit Asavanant [1,*] Kosuke Fukui [1,†] Atsushi Sakaguchi [2,‡] and Akira Furusawa [1,2,§]

[1]*Department of Applied Physics, School of Engineering, The University of Tokyo, 7-3-1 Hongo, Bunkyo-ku, Tokyo 113-8656, Japan*
[2]*Optical Quantum Computing Research Team, RIKEN Center for Quantum Computing, 2-1 Hirosawa, Wako, Saitama 351-0198, Japan*

Optical switches and rerouting networks are considered essential in optical quantum computers where they are used for injection and dejection of the necessary quantum states into an optical quantum computer. Practical optical switches and rerouting networks are, however, experimentally challenging as they must have extremely low loss, small switching time, high repetition rate, and minimum optical nonlinearity, requirements that are difficult to achieve simultaneously. In this paper, we present an optical quantum computation platform that does not require such optical switches. Our method is based on continuous-variable measurement-based quantum computation where, instead of the typical cluster states, we modify the structure of the quantum entanglement, so that the quantum teleportation protocol can be employed instead of optical switching and rerouting. The quantum entanglement structure in our architecture has additional modes that allow quantum states to be teleported in or out of the computation along the cluster state, a task that normally requires optical switches. We also outline how to combine our platform with Gottesman-Kitaev-Preskill encoding, the currently most promising encoding for a continuous-variable system.

I. INTRODUCTION

Optical systems are promising candidates for quantum computation as they can be implemented at room temperature and atmospheric pressure, and have high compatibility with optical communications. Optical quantum computation can be largely categorized into two types: discrete variable (DV) and continuous variable (CV). Various researches have been done for both types and many different architectures have been theoretically developed and experimentally demonstrated [1,2]. One of the approaches that has shown a great potential toward large-scale quantum computation is the time-domain CV measurement-based quantum computation [3]. In this platform, a large-scale universal computational resource—the cluster state [4,5]—has been generated [6–9] and basic operations on these scalable platforms have also been realized [10,11]. In addition to the time-domain encoding, CV frequency-domain encoding [12,13] and spatial-mode encoding [14,15] also hold promising potential toward large-scale quantum computation.

Regardless of the details of each optical platform, the optical switch is considered a key component in both DV

[16,17] and CV [18–21] architecture. The main functionality of optical switches is changing the path of the optical beams. They are used in many tasks in the optical quantum computation such as injection and dejection of the quantum states into and out of the computation platform, and multiplexing of the quantum light sources. Although there are some proof-of-principle experiments regarding the optical switches for quantum computation [18–21], realizing practical optical switches for quantum computation remains challenging. This is because optical switches for optical quantum computation must have low optical losses, high switching speed, high repetition rate, and compactness—requirements that tend to be incompatible. High switching speed and repetition rate is required to harness the speed of the optical quantum computation [1], while the compactness is important when considering integration of the system. The current candidates for the optical switches such as a Pockels cell [22] and a highly nonlinear medium [23] satisfy only partial requirements. Therefore, we need to find a solution to the optical switch to realize full-fledged quantum computation.

In this paper, we present a theoretical solution to this problem: an optical quantum computation architecture that does not require optical switches. Our architecture is based on the CV measurement-based optical quantum computation in the time domain using cluster states. But instead of the usual cluster state, we add additional light modes that are entangled to the cluster states. These modes can be considered roughly equivalent to the input or output of the optical switches. The process of the switching, which usually utilizes an optical nonlinear medium, is done by changing the basis of the measurements of these additional modes, allowing us to control where to teleport (or not to teleport at all) the input to. Switching of the basis of the measurement in the CV

---

*warit@alice.t.u-tokyo.ac.jp
†fukuik.opt@gmail.com
‡atsushi.sakaguchi@riken.jp
§akiraf@ap.t.u-tokyo.ac.jp

measurement-based optical quantum computation has been recently demonstrated [10,11], meaning that our architecture only requires modification of the quantum entanglement structure, without introducing any new element to replace the optical switches. We analyze the performance of our architecture when it is combined with the Gottesman-Kitaev-Preskill (GKP) qubit [24–27]—the currently most promising logical qubit—using the Knill-type correction [28]. Removing the necessity of the optical switching from the optical quantum computation platform makes our architecture unique compared to the other time-domain-based CV architecture [8,9,20,21].

This paper is structured as follows. Section II explains preliminaries and notations used in this paper. The proposed setup and its analysis are shown in Sec. III. Section IV discusses the experimental feasibility and Sec. V concludes the paper.

II. PRELIMINARIES

First we explain the basic notations and review the concepts of CV measurement-based quantum computation.

A. Notations

In the CV quantum computation, the physical quantities of our interest are quadratures. Quadratures are denoted by operators $\hat{x}$ and $\hat{p}$ which satisfy $[\hat{x}, \hat{p}] = i$ (which corresponds to $\hbar = 1$). The quadrature operators are related to annihilation operator $\hat{a}$ and creation operator $\hat{a}^\dagger$ via

$$\hat{x} = \frac{1}{\sqrt{2}}(\hat{a} + \hat{a}^\dagger), \tag{1}$$

$$\hat{p} = -\frac{i}{\sqrt{2}}(\hat{a} - \hat{a}^\dagger). \tag{2}$$

Next, we define some of the basic operations in this paper. First, a squeezing operator $\hat{S}(r)$ with a squeezing parameter r transforms the quadrature operators in the Heisenberg picture as

$$\hat{S}^\dagger(r)\begin{pmatrix} \hat{x} \\ \hat{p} \end{pmatrix}\hat{S}(r) = \begin{pmatrix} e^r & 0 \\ 0 & e^{-r} \end{pmatrix}\begin{pmatrix} \hat{x} \\ \hat{p} \end{pmatrix}. \tag{3}$$

Another important operation is a phase rotation $\hat{R}(\theta)$ which transforms quadrature operators as

$$\hat{R}^\dagger(\theta)\begin{pmatrix} \hat{x} \\ \hat{p} \end{pmatrix}\hat{R}(\theta) = \begin{pmatrix} \cos\theta & \sin\theta \\ -\sin\theta & \cos\theta \end{pmatrix}\begin{pmatrix} \hat{x} \\ \hat{p} \end{pmatrix}. \tag{4}$$

Regarding two-mode operation, we first consider beam splitter interaction $\hat{B}_{12}(\sqrt{R})$ which we define as

$$\hat{B}_{12}^\dagger(\sqrt{R})\begin{pmatrix} \hat{x}_1 \\ \hat{x}_2 \\ \hat{p}_1 \\ \hat{p}_2 \end{pmatrix}\hat{B}_{12}(\sqrt{R})$$

$$= \begin{pmatrix} \sqrt{R} & \sqrt{1-R} & 0 & 0 \\ -\sqrt{1-R} & \sqrt{R} & 0 & 0 \\ 0 & 0 & \sqrt{R} & \sqrt{1-R} \\ 0 & 0 & -\sqrt{1-R} & \sqrt{R} \end{pmatrix}\begin{pmatrix} \hat{x}_1 \\ \hat{x}_2 \\ \hat{p}_1 \\ \hat{p}_2 \end{pmatrix}. \tag{5}$$

Another two-mode operation which will be used in this paper is a CV version of the controlled-Z gate, denoted by $\hat{C}_Z$. We will consider a control-Z gate with gain of 1, which transforms the quadrature operators as

$$\hat{C}_Z^\dagger\begin{pmatrix} \hat{x}_1 \\ \hat{x}_2 \\ \hat{p}_1 \\ \hat{p}_2 \end{pmatrix}\hat{C}_Z = \begin{pmatrix} 1 & 0 & 0 & 0 \\ 0 & 1 & 0 & 0 \\ 0 & -1 & 1 & 0 \\ -1 & 0 & 0 & 1 \end{pmatrix}\begin{pmatrix} \hat{x}_1 \\ \hat{x}_2 \\ \hat{p}_1 \\ \hat{p}_2 \end{pmatrix}. \tag{6}$$

B. Quantum entanglement and quantum computation

It is known that quantum entanglements with appropriate structures, i.e., the cluster states, allow universal quantum computation when combined with local (single mode or single qubit) measurements and feedforward operations that depend on the measurement results [4,5]. Quantum computation using cluster states can be equivalently considered as sequential quantum teleportation where the measurement bases are chosen depending on the desired operations [6].

Quantum entanglement (and pure Gaussian states in general) in a CV system is defined by a set of operators called nullifiers. For a N-mode pure Gaussian state $|G\rangle$, an operator $\hat{\delta}$ is a nullifier of $|G\rangle$ if and only if

$$\hat{\delta}|G\rangle = 0 \tag{7}$$

and the state $|G\rangle$ can be uniquely defined by N independent nullifiers.

In the generation of many ideal CV quantum entanglements, including the cluster states, infinite squeezing is required. In actual physical situations, however, we can only achieve finite squeezing. The imperfections due to the finite squeezing appear as the nonzero variances of the nullifiers. When CV quantum entanglements are used, especially in measurement-based quantum computation, the nonzero variances of the nullifiers determine the imperfections of the computation and appear as Gaussian noises in the output mode. Note that in the absence of phase fluctuations this noise is determined by only the squeezing component of the squeezed states used in the generation of the entanglement and not the antisqueezing components as the contributions from the antisqueezing components are erased by the feedforward operations [29]. These characteristics make the variances of the nullifiers useful as a primary figure of merit in the CV measurement-based quantum computation.

C. Time-domain multiplexing method and optical switches

In the quantum computation based on the cluster state, the size of the cluster state determines the possible size of the computation. Thus, it is important that a large-scale cluster state can be generated. In the conventional optical setting, CV cluster states are generated by interfering multiple squeezed lights where each squeezed light source corresponds to a mode of the cluster state. This method, however, lacks scalability as the number of the required components scales with the size of the cluster state.

To achieve scalability, generation of the CV cluster states via multiplexing has been widely researched. Here we will introduce the methodology called time-domain
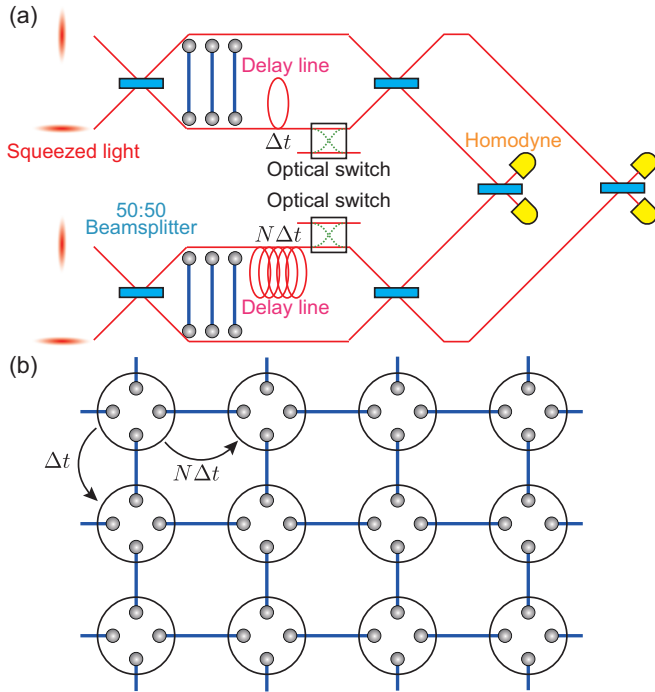
FIG. 1. Schematic diagram of the time-domain-multiplexed quad-rail lattice cluster state setup. (a) The setup which consists of four squeezed light sources, five beam splitters, four homodyne detectors, and optical switches. Note that there are only two optical switches in the figure, but in an actual situation where we have to multiplex the non-Gaussian state sources we would require many more optical switches, depending on the level of multiplexing. (b) Macronode representation of the quad-rail lattice cluster state where the two-mode entanglement shown is the two-mode squeezed state (the Einstein-Podolsky-Rosen state in the infinite squeezing limit). Each node corresponds to a temporal wave packet of a width Δt. A switch for implementation of error correction is also required but it is omitted from the figure [30].

multiplexing, which will also be the basis of our architecture. Figure 1 shows an experimental setup of the time-domain measurement-based quantum computation using a type of two-dimensional cluster state called the quad-rail lattice (QRL) [3]. In the time-domain multiplexing method, instead of considering a single beam as a single mode, we consider multiple time-bin wave packets of temporal width Δt that are multiplexed on the same beam. By using the optical delay lines with appropriate lengths, these wave packets can be entangled into a large scale cluster state. In addition to the QRL, there are cluster states with different structures that have been shown to be universal resources for quantum computation [8,9,19].

The quantum computation using the QRL (and other CV cluster states) can be considered equivalent to the quantum teleportation protocol where the two-mode squeezed states are measured using a network of linear optics and homodyne measurements [31]. As the cluster state and homodyne measurement can realize only Gaussian operations, we also need the non-Gaussian elements [32]. The non-Gaussian elements can be added to the cluster states either as input states or by replacing some of the squeezed states with non-Gaussian

states [21], or by replacing the homodyne detector with a non-Gaussian measurement gadget [19]. Regardless of the approach we choose, optical switches are needed to implement these tasks. In Fig. 1, we show optical switches for injection of the input states in the setup of the QRL. If we consider quantum error correction (QEC) using a GKP qubit, we also need additional switches for switching between computation using a cluster state and a QEC gadget [19]. In the case that the Knill-type error correction (which we will explain more in Sec. III D) is used, we need optical switches for switching between the initial squeezed lights and the ancillary qunaught states [21] (see also Appendix 2). In a more practical consideration, as the non-Gaussian states are generated probabilistically in the optical system, a switching tree of a circuit depth of $\log_2 M$ depth is required for multiplexing M sources with an additional switch for injecting the state into the architecture.

The optical switch plays an important role not only in the time-domain multiplexing method, but in almost every optical quantum computation architecture. For the optical switches to be useful in optical quantum computation they must satisfy various requirements. First, optical switches must have low optical losses so that they can handle quantum states as we see in Fig. 1. Second, in Fig. 1, the clock frequency of the optical quantum computer is determined by the size of the wave packet (denoted as Δt); the smaller the wave-packet size is, the more information we can pack. Thus, the optical switches must have high switching speed and high repetition rate so that we can pack the wave packets close to each other, making Δt small. Third, the optical switch should not affect the quantum states passing through the switch. Although this requirement seems to be easily achieved, this is not necessarily the case as most of the optical switches utilize nonlinear an optical medium for fast switching.

III. MAIN RESULTS

A. Proposed setup

To circumvent the needs of the optical switching, we propose a setup shown in Fig. 2. In this setup, we replace the two-mode squeezed states in Fig. 1 with a CV quantum entanglement that has a tree graph structure branching out at both ends (Fig. 3)—which we will call a *two-sided tree graph*. The nullifiers of the two-sided tree graph are given by

$$\hat{\delta}_1 = \hat{p}_1 - \hat{x}_2 - \sum_{k \in \mathcal{K}} \hat{x}_k, \qquad (8)$$

$$\hat{\delta}_2 = \hat{p}_2 - \hat{x}_1 - \sum_{l \in \mathcal{L}} \hat{x}_l, \qquad (9)$$

$$\hat{\delta}_k = \hat{p}_k - \hat{x}_1, \qquad (10)$$

$$\hat{\delta}_l = \hat{p}_l - \hat{x}_2, \qquad (11)$$

where $\mathcal{K}$ ($\mathcal{L}$) is a set of nodes that is connected to mode 1 (2) and does not include mode 2 (1). Note that it is possible to transform this state into a state whose nullifiers are composed of only quadrature operator $\hat{x}$ or $\hat{p}$. Such a type of state is the called $\mathcal{H}$-graph which can be generated via appropriate generalized parametric down conversion.
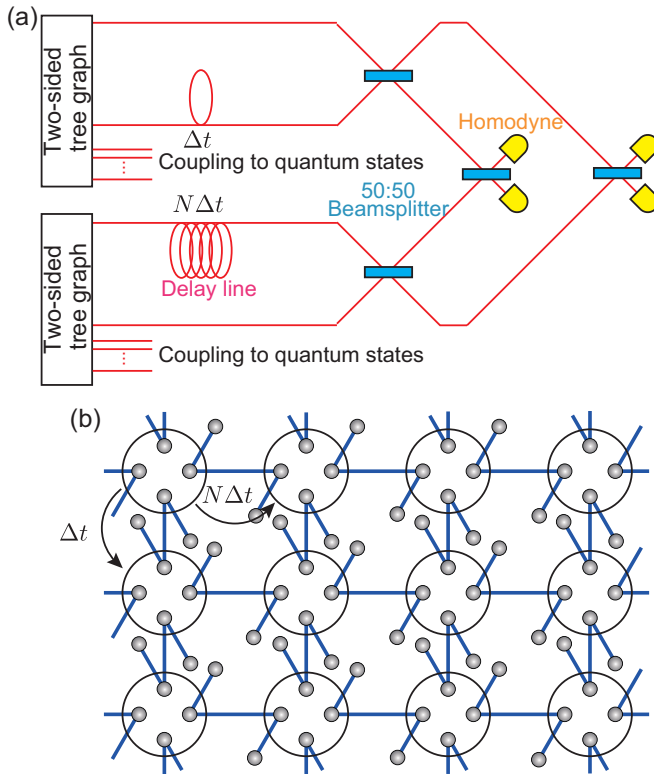
FIG. 2. Proposed switching-free optical quantum computer setup. (a) Experimental setup. (b) Macronode representation of the quantum entanglement generated from the setup in (a). For simplicity, we show the case with four modes.

The modes in set $\mathcal{K}$ and $\mathcal{L}$ (which we will be referring to as the branches of the two-sided tree graph states) are then coupled to the ancillary quantum states we wish to inject to the cluster states, while mode 1 and mode 2 act as modes for quantum computation. Figure 3(b) shows an example of a possible generation setup of the two-sided tree graph in the four-mode case. This is the case with the smallest number of modes and the resource state becomes a four-mode linear cluster state which has already been experimentally demonstrated [33]. For a case with more modes, it has been theoretically shown that arbitrary Gaussian states can be generated with offline squeezing and linear optics [34], meaning that we
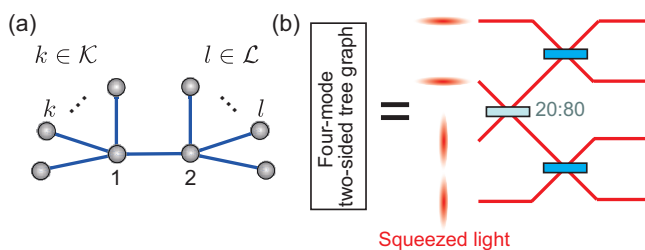

FIG. 3. Two-sided tree graph state. (a) General graphical structure. The mode connected to mode 1 (mode 2) is denoted by the index k (l) and is an element of a set $\mathcal{K}$ ($\mathcal{L}$). (b) A generation setup of a four-mode two-sided tree graph state using offline squeezing and linear optics.

can definitely find a physical circuit that realizes this initial resource state.

The ideal two-sided tree graph states require infinite squeezing to generate. In the actual situation, we generate states that approach the ideal two-sided tree graph states in the infinite squeezing limit. There are, however, various possible setups that asymptotically approach the same states, meaning that the details of the noises in the actual system will depend on the generation method. Here we will consider the situation that aligns with actual experiments: the case where the two-sided tree graph states are generated using linear optics and offline squeezed states with the same squeezing parameter r using the method in Ref. [34].

In this generation method, the nullifiers will only possess the squeezing components, ensuring that they tend to zero in the infinite squeezing limit. Regardless of the details of the linear optics used in the generation circuit, the variances of the nullifiers will become

$$\mathrm{Var}(\hat{\delta}_1) = (K + 2)\sigma^2, \tag{12}$$

$$\mathrm{Var}(\hat{\delta}_2) = (L + 2)\sigma^2, \tag{13}$$

$$\mathrm{Var}(\hat{\delta}_k) = \mathrm{Var}(\hat{\delta}_l) = 2\sigma^2, \tag{14}$$

where $K(L)$ is the number of the modes in the branches, i.e., the number of the elements in set $\mathcal{K}$ ($\mathcal{L}$), and σ^2 is the variance of the offline squeezed states used in the generation, given by $\sigma^2 = e^{-2r}/2$. Another way to think about the above equations is that with the generation method in Ref. [34], if we input vacuum states into the beam splitter network, we will simply get the vacuum state out; as such the variance of the nullifiers in the above equation should simply become the sum of vacuum variance. The variances of the nullifiers determine the imperfectness of the computation when the resource states are used.

B. Input state injection and rerouting

Here we first discuss how the two-sided tree graph state can be used for state injection and rerouting. Figure 4 shows the schematic diagram of how to inject the quantum state using quantum teleportation and the branches of the two-sided tree graph state. For the optical quantum computation, as most of the proposed generation schemes for the non-Gaussian states that are required for universal quantum computation are probabilistic, multiplexing of the state generators is required to make the whole system semideterministic. Moreover, there are various instances in which we might want to inject different types of quantum states that are generated from different sources into the cluster state. In the conventional methods, these tasks are done by optical switches and a rerouting network. Below, we will show how our architecture replaces them with quantum teleportation.

As it is shown in Fig. 4, if we implement joint measurement between the mode on the branch and the mode of the state we want to inject using different measurement bases, the quantum state will be teleported into the mode that is used in the computation (with a possibility of an additional Gaussian unitary as the teleportation circuit can be used to implement a Gaussian unitary [35]). On the other hand, what
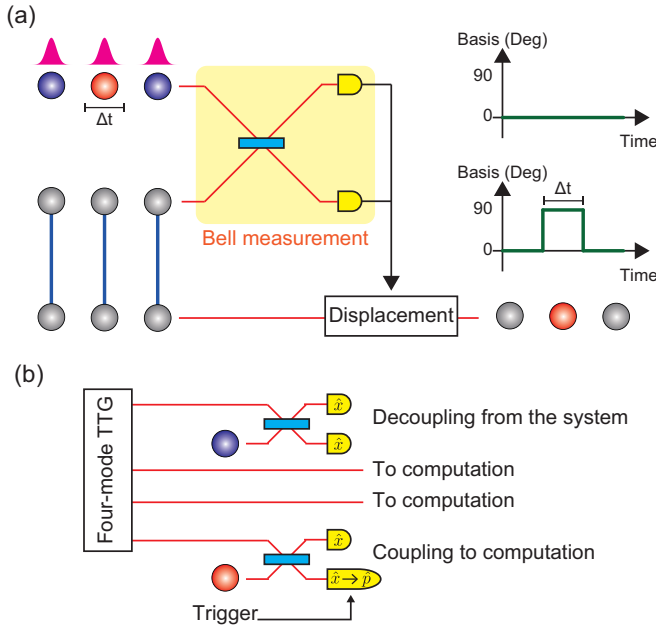
FIG. 4. Quantum teleportation and state injection. (a) Selective quantum teleportation. Here we dynamically change the measurement bases and the feedforward operation so that only the desired mode (red mode) is teleported, while the modes we want to block (purple modes) are not teleported to the output. We assume that the measurement bases for blocking the blue modes are x bases, although they can be any same bases in general. A measurement of $0°$ corresponds to the x basis, while $90°$ corresponds to the p basis. (b) Application of quantum teleportation to state injection. Here, the generation of the desired quantum state triggers the switching of the measurement basis. This trigger could be, for example, successful in photon detection in the heralding method.

is important is what happens when the measurement bases of the joint measurement are the same. From Fig. 4(a), we suppose that both modes are measured with the x basis for the modes we wanted to block (the purple modes). Then, we can write down the relationship between quadrature operators and the measurement results as

$$m_{A'} = \frac{1}{\sqrt{2}}(\hat{x}_A + \hat{x}_B), \tag{15}$$

$$m_{B'} = \frac{1}{\sqrt{2}}(\hat{x}_B - \hat{x}_A). \tag{16}$$

Inverting these equations, we have

$$\hat{x}_A = \frac{1}{\sqrt{2}}(m_{A'} - m_{B'}), \tag{17}$$

$$\hat{x}_B = \frac{1}{\sqrt{2}}(m_{A'} + m_{B'}). \tag{18}$$

This shows that measuring two modes with the same bases after a beam splitter is equivalent to measuring each mode separately. Therefore, by selecting the same measurement bases after the beam splitter, we are effectively measuring each mode separately, preventing the quantum state from being teleported into the cluster state. From the nullifiers in Eqs. (8)–(11), we can also see that measuring the quadrature x corresponds to erasing the measured node from the

two-sided tree graph state without affecting other nodes. As such, by changing the measurement bases and the feedforward operation dynamically, we can select which temporal modes on the input should be teleported, while blocking the other modes. Figure 4(b) shows how to use this in our architecture. When the state is generated, the measurement base of the corresponding homodyne detector is changed from x to p and the state is teleported into the cluster state. When the desired state is not generated, the measurement bases remain x bases and disjoint the undesirable mode from the computation without affecting the other modes. As our resource states will have finite squeezing in the actual setting, there will be imperfection related to the state injections. This imperfection increases as the number of the modes of the two-sided tree graph state increases and we give the detailed analysis results in Sec. IV.

Switching of the measurement basis, which is a technique required for this method, can be done by changing the phase of the local oscillator of the homodyne detector. Experimentally, this dynamical phase changing of the local oscillator for measurement of the cluster state has been experimentally demonstrated [10,11]. We can also perform state dejection into the modes on the branches in a similar manner to the state injection.

C. Universality

Figure 5 shows how to implement universal quantum computation on our architecture. To realize universal CV operations, we need to be able to implement an arbitrary multimode Gaussian operation and any single non-Gaussian operation [32]. Since the two-sided tree graph state can be reduced to a two-mode cluster state [Fig. 5(a)], the implementation of the Gaussian operations follows the protocol of the QRL cluster state [31] and can be done with homodyne measurements and feedforward operations.

On the other hand, there are several ways non-Gaussian operations can be implemented. Here we first consider a cubic phase gate whose unitary operator is given by $\hat{U}_{CPG}(\gamma) = \exp(i\gamma\hat{x}^3)$, where γ is the strength of the operation. The most basic way would be implementation by replacing one of the homodyne detectors with cubic phase measurement [19]. This, however, requires optical switching to switch between the homodyne measurement and cubic phase measurement. Figures 5(b)–5(d) show how to implement the cubic phase gate without utilizing the optical switch. This method is an application of the gate teleportation protocol [37]. In this approach, we use the mode of the two-sided tree graph to teleport the cubic phase state into the cluster state [Fig. 5(b)]. The resulting entangled state is equivalent to the usual two-mode entanglement for quantum teleportation with the cubic phase gate acting on one of the modes [Fig. 5(c)]. Then, the cubic phase gate is implemented by teleporting the input state through the resulting two-mode entangle state [Fig. 5(d)]. We note here that the required feedforward operation will change from a displacement operation to a Gaussian operation, which can be done using the cluster state.

When we consider fault-tolerant quantum computation, it is important to consider how to implement a universal logical gate set on the GKP qubits, which is currently the most
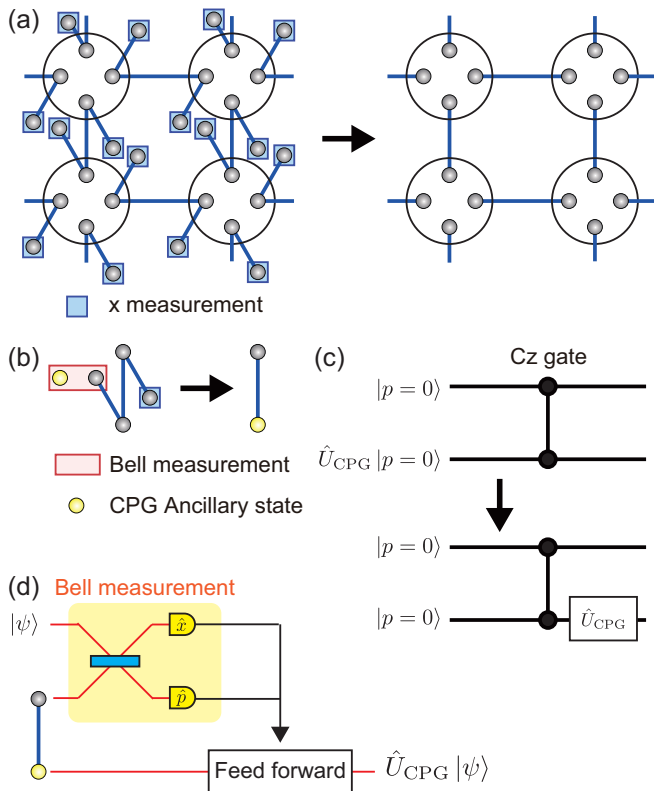
FIG. 5. Quantum computation using the proposed setup. (a) x measurement on the branches of the two-sided tree graph reduces the state to the QRL cluster state, allowing implementation of arbitrary multimode Gaussian operations. (b) Generation of entanglement for implementing the cubic phase gate (CPG) by teleporting the CPG ancillary state $|\psi_{\mathrm{CPG}}\rangle = \exp(i\gamma\hat{x}^3)|p=0\rangle$ into the cluster state. (c) Equivalence between the resulting non-Gaussian entanglement and the two-mode entanglement for quantum teleportation with CPG implemented on one of the modes. (d) CPG via quantum teleportation with the non-Gaussian entanglement. We note that the feedforward operation here is in general a Gaussian operation.
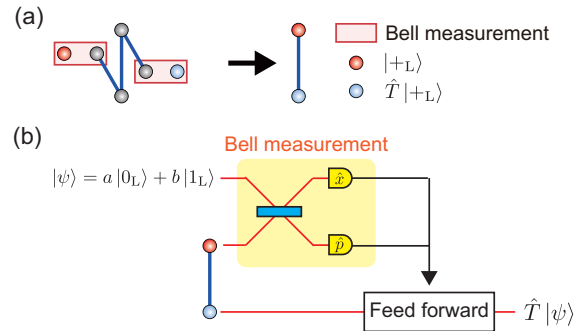

FIG. 6. Non-Clifford gate on GKP using gate teleportation on our setup. (a) Generation of the required resource state by teleporting GKP logical $|+_{\mathrm{L}}\rangle = (|0_{\mathrm{L}}\rangle + |1_{\mathrm{L}}\rangle)/\sqrt{2}$ and $\hat{T}|+_{\mathrm{L}}\rangle$ in the the two-sided tree graph state. $\hat{T}$ is a non-Clifford gate which transforms a quantum state as $a|0_{\mathrm{L}}\rangle + b|1_{\mathrm{L}}\rangle \rightarrow a|0_{\mathrm{L}}\rangle + b\exp(i\pi/4)|1_{\mathrm{L}}\rangle$. (b) Quantum teleportation through this new resource allows implementation of $\hat{T}$. Note that the feedforward operation here is a Gaussian operation.

D. Error syndrome measurement and correction

In this section, we will discuss how to implement QEC in our architecture. As we have outlined in Sec. III B, the branches on the sides of the two-sided tree graph states can be used to teleport and inject various quantum states, changing the two-mode entangled states of the QRL into the quantum entanglement that is required for each application. This property makes our architecture goes well with Knill-type QEC [28] which will be the QEC scheme we consider in this paper. Knill-type QEC is implemented by quantum teleportation of the logical qubits through a fresh logical Bell state. The Knill-type QEC for the GKP qubit has been investigated in Refs. [40,41].

Figure 7 shows the implementation of the Knill-type QEC for our architecture. We first generate GKP logical $|+_L\rangle$, then teleport it into the two-sided tree graph states. As the CV controlled-Z gate is also a logical controlled-Z gate for the GKP qubit, this results in the two-mode GKP Bell state (up to local Pauli gates) which is a resource entanglement required in the Knill-type QEC. Then, as shown in Fig. 7(b), the data qubit is teleported through this GKP Bell state. The error correction is implemented by the displacement operations depending on the results of the homodyne measurements.

As the generation of the required GKP ancillary states is usually probabilistic in the optical systems, there is a possibility that both ancillary states are not simultaneously generated and only one of the ancillary states is teleported into the cluster state. Even then, the resulting entanglement can be used to correct one of the quadratures and we can repeat the process until both quadratures are corrected [40]. The success rate of this repeat-until-success approach can be increased by increasing the number of the modes in the two-sided tree graph states, which allow the multiplexing of the generation of the GKP ancillary states. Note that in the quadrail lattice, two data qubits can be corrected simultaneously as shown in Fig. 7(c). To quantify the performance of our setup, we consider the implementation of the $\hat{F}\hat{F}\hat{C}_Z$ using our architecture and numerically calculate the error probability

promising encoding of the CV system. In GKP qubit encoding, Clifford operations can be implemented using Gaussian operations, while the implementation of the non-Clifford operation requires non-Gaussian operations [24]. For Clifford operations, we can use the strategy for implementing Gaussian operations as outlined in this section. It has also been shown in the original GKP qubit proposal that the cubic phase gate can be used to implement non-Clifford operation. It has been pointed out, however, that this method might not be the most optimum method to implement non-Clifford operation on the GKP qubit [38]. Another method to implement the non-Clifford operations on the GKP qubit is to use gate teleportation methodology [39]. Our architecture can implement this non-Clifford operation by using the modes of the two-sided tree graph to teleport the ancillary state required and modify the two-sided tree graph states into the required resource states shown in Fig. 6. Note that the required feedforward operations in both methodologies are Gaussian operations which can be implemented easily on our architecture.
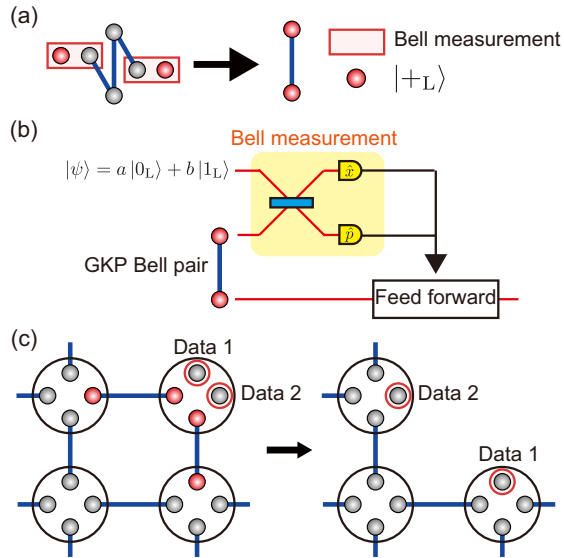
FIG. 7. Knill-type quantum error correction for our setup. (a) Generation of the GKP Bell pair by teleporting $|+_L\rangle$ into the two-sided tree graph state. (b) Knill-type quantum error correction by teleporting the GKP-encoded state through the GKP Bell pair. The feedforward operation here is a displacement operation. (c) Simultaneous quantum error correction of the data qubit by using the structure of the entanglement in our setup.

when Knill-type QEC is employed. See the Appendix for the details of the numerical analysis. Figure 8 shows the error probability of the $\hat{F}\hat{F}\hat{C}_Z$ gate with the switching-free setup for several N which are numbers of the branch on each side of the two-sided tree graph (i.e., the graph as $2N + 2$ modes). In this graph, we assume that the squeezing level of the squeezed vacuum and the squeezing of the GKP peaks are related via $\sigma^2 = \exp(-2r)/2$, where r is the squeezing parameter of the squeezed vacuum state. This implies that our method, when combined with a qubit error correction code for correcting qubit errors induced by GKP correction, can provide fault-tolerant quantum computation even for a large N if adequate squeezing can be achieved. As a reference, we
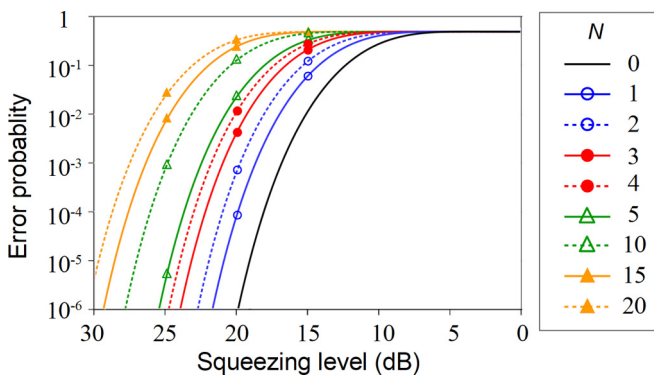

FIG. 8. The error probability of the $\hat{F}\hat{F}\hat{C}_Z$ gate of the proposed method with the switching-free setup. N denotes the number of branches on one side of the two-sided tree graph state. As a reference, we also plot an ideal Knill-type QEC (the solid black line) dependence on squeezing level.

also perform similar calculation of the Knill-type QEC using optical switches and the details are shown in the Appendix.

IV. EXPERIMENTAL FEASIBILITY

In this section, we will discuss the experimental feasibility of our architecture. First, we discuss how large the number of modes N on each side of the two-sided tree graphs must be. The required number of N depends on various factors. If the state generator we consider can only generate a single type of states, then the number of N must, at the very least, be equal to the number of the types of the quantum states needed in the actual computation. Even if our state generator can implement generation of various quantum states, there are situations where we would want N to be more than 1. For example, we would want a large N to compensate for the probabilistic generation using the heralding method. In the method using the optical switch, a switching network of a circuit depth $\log_2 N$ is required in the multiplexing of N sources of non-Gaussian states, meaning that the number of the mode on each side of the two-sided tree graph can be roughly translated to the number of required optical switches in the conventional method. As an example, if we want to generate a GKP Bell pair with the success probability of 99.99%, the success preparation probability of the GKP qubit must be above 94.5, 73.5, 56.0, and 45.5% for $N = 5, 10, 15$, and 20, respectively. From Fig. 8, as N increases, the error probability also increases. This is due to the fact that the unused modes are disentangled from the computation via measurements. There might exist a more efficient methodology along the same idea of using the quantum teleportation circuit as an optical switch and we leave the exploration of such an idea to a future work.

Regarding the experimental feasibility, despite the fact that it is possible to make a free-space optical switch with bulk optics where the losses are limited mainly by the quality of the antireflection coating, free-space optics are not a good choice when considering long term stability, reproducibility, and integrability. This is especially true when we consider the routing network for the non-Gaussian ancillary state, where the routing network would be composed of multiple optical switches. For the integrated optics such as silicon photonics, the optical losses are still too high for the quantum applications [42].

On the other hand, in the approach of using entanglement in this paper, the CV quantum entanglement can be generated using only offline squeezed lights and passive linear optics, while the switching of the measurement bases is done by changing the phases of the classical local oscillators which do not have the severe requirements regarding optical losses. In principle, the generation of the required quantum entanglement in the time domain with sufficient quality is possible by extending the technology used in the cluster state generation and computation [8–11] and inclusion of a high-quality squeezed light source [43]. Regarding the preparation of the GKP qubit which is required in most of the optical quantum computation architecture, although there are recent realizations in the ion-trapped system [44] and superconducting system [45] and the optical generation has not been achieved yet, there are a few promising theoretical proposals (see, for example, Refs. [46–48]). Also, development of optical

quantum memory capable of storing a multiphoton quantum state such as the GKP state is being developed [36,49].

V. CONCLUSION

We have presented an optical quantum computation platform which removes the necessity of the optical switches. Our approach incorporates the possibility of multiplexing of multiple non-Gaussian ancillary state generators by using the quantum teleportation protocol via two-sided tree graph states and is compatible with the teleportation-based QEC. The physical realization of our system is also highly scalable as it is compatible with the time-domain multiplexing methodology, and the only active component necessary is the phase modulation of the local oscillators, which is relatively easy as modulation of classical light is a well-established technology. Hence, this architecture shows a possibility of optical quantum architecture that does not require inline optical switching.

ACKNOWLEDGMENTS

APPENDIX: ANALYSIS METHOD

In this section, we describe the methodology used in the analysis of the quantum gate on the QRL using the conventional method with optical switching and the proposed method.

1. Quantum gate on the QRL

First, we describe general implementation of the gate using the cluster state with nonunity edge weight as described in Ref. [30]. Then, we will explain the feature of the QRL and our method which allows us to implement the gate as if the edge weight is unity. The single-mode quantum gate in each step of quantum computation (QC) using the QRL with nonunity edge weight has the form

$$\hat{U} = \hat{S}(s)\hat{R}\left(\frac{\theta_+}{2}\right)\hat{S}\left(\tan\frac{\theta_-}{2}\right)\hat{R}\left(\frac{\theta_+}{2}\right), \tag{A1}$$

where $\theta_\pm$ is the linear combination of the measurement bases of the homodyne measurement, and s is a squeezing parameter that depends on the edge weight t of the two-mode squeezed vacuum state as $e^s = 1/t$. In this gate implementation, an additional step of QC has to be implemented to compensate for the effects of $\hat{S}(s)$ for some gates. For example, the Fourier gate $\hat{F} = \hat{R}(\pi/2)$ using the two-mode squeezed vacuum with the edge weight t requires two computational steps to compensate and cancel out the squeezing gate $\hat{S}(s)$. In the first computational step, the quantum gate $\hat{U}_1 = \hat{S}(s)\hat{F}$ is implemented by selecting $\theta_+ = \pi/2$ and $\theta_- = 0$. In the second step, we implement the squeezing gate $\hat{U}_2 = \hat{S}(-s)$. Overall, this results in the Fourier gate $\hat{U}_2\hat{U}_1 = \hat{S}(-s)\hat{S}(s)\hat{F} = \hat{F}$.
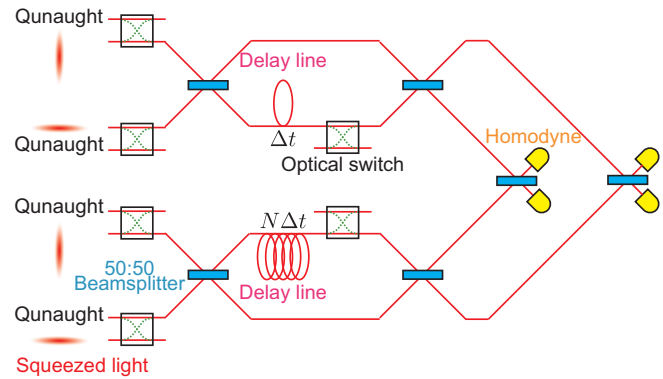

FIG. 9. Schematic diagram of the time-domain-multiplexed quad-rail lattice cluster state setup for the Knill-type QEC, where optical switches are set before first beam splitters and the Knill-type QEC is implemented by the GKP-Bell pair. The GKP-Bell pair is generated by 50:50 beam splitter coupling between two input qunaught states. Note that in the calculation we ignore the optical losses due to the optical switches after the two optical delay lines as these losses are related mainly to the input state injection, rather than Knill-type QEC.

For the QRL and our setup, as the generated states belong to one of a class of states called the $\mathcal{H}$-graph state, it is known that we can implement the single-mode quantum gate using quantum teleportation [31]. The form of the gate in this case is

$$\hat{U} = \hat{R}\left(\frac{\theta_+}{2}\right)\hat{S}\left(\tan\frac{\theta_-}{2}\right)\hat{R}\left(\frac{\theta_+}{2}\right). \tag{A2}$$

Thanks to the edge-weight parameter, the Fourier gate requires only a single computational step with $\theta_+ = \pi/2$ and $\theta_- = 0$.

2. Knill-type QEC with an optical switch

In this section, we describe the implementation of the $\hat{F}\hat{F}\hat{C}_z$ gate using the Knill-type QEC with optical switches and calculate its error probability as a comparison to our method. Figure 9 shows a schematic diagram of the setup. In this setup, there is an optical switch on each path before the first beam splitter coupling. These optical switches are used for switching between the squeezed state and the ancillary state for the Knill-type QEC. We add optical switches in all four paths so that the simultaneous QEC of two data bits as shown in Fig. 7(d) would also be possible in this setup. In the Knill-type QEC, the required GKP Bell pairs are prepared as the two-mode entanglement for the macronode in the QRL cluster state. This is done by switching from the squeezed states to the qunaught state given by $\sum_{m=-\infty}^{\infty} |2m\sqrt{2\pi}\rangle_q$. By interfering the qunaught state with a beam splitter, a GKP Bell pair is generated. Then, the logical information is teleported through this GKP Bell pair and the Knill-type QEC is implemented. We note that this process corresponds to the qubit quantum teleportation using the GKP Bell pair instead of the CV quantum teleportation using the two-mode squeezed state.
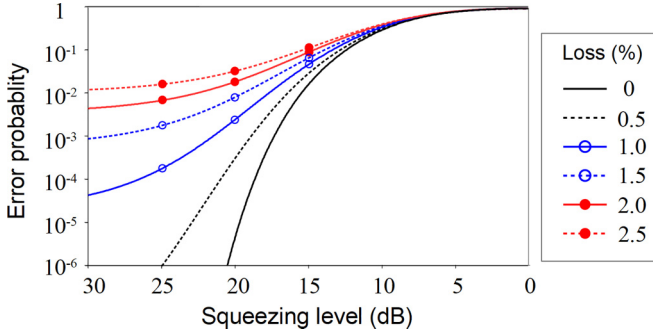
FIG. 10. The error probability of the $\hat{F}\hat{F}\hat{C}_z$ gate using the Knill-type QEC with the optical switching for several η_{in}.

Next, we consider the effects of the optical switch on the squeezed vacuum state. The optical switch transforms the variances of the squeezed vacuum state as

$$\sigma_{\text{in},x}^2 \rightarrow \eta_{\text{in}}\sigma_{\text{in},x}^2 + \frac{1-\eta_{\text{in}}}{2}, \qquad \text{(A3)}$$

$$\sigma_{\text{in},p}^2 \rightarrow \eta_{\text{in}}\sigma_{\text{in},p}^2 + \frac{1-\eta_{\text{in}}}{2}, \qquad \text{(A4)}$$

where $\sigma_{\text{in},x}^2$ ($\sigma_{\text{in},p}^2$) is the variance of the x (p) quadrature of the initial squeezed vacuum state before an optical switch, and η_{in} is the efficiency of the optical switch. From this variance, we can obtain the edge-weight and self-loop parameter of the resulting two-mode entanglement [50], $t = \tanh^2(2r)$ and $i\epsilon = i\,\text{sech}(2r)$, where the squeezing parameter r is derived from the relation

$$\frac{1}{2}e^{-2r} = \eta_{\text{in}}\sigma_{\text{in},x(p)}^2 + \frac{1-\eta_{\text{in}}}{2}. \qquad \text{(A5)}$$

Hence, the variance of the squeezed vacuum state becomes larger due to the optical switch.

We can also calculate the effects of the optical switches on the GKP Bell pair. As the optical loss affects the codewords of the GKP qubits, the qunaught state needs to be amplified using the preamplification technique prior to passing through the optical switches (see Appendix 4). Thus, the variances are transformed as

$$\delta_{\text{in},x}^2 \rightarrow \delta_{\text{in},x}^2 + 1 - \eta_{\text{in}}, \qquad \text{(A6)}$$

$$\delta_{\text{in},p}^2 \rightarrow \delta_{\text{in},p}^2 + 1 - \eta_{\text{in}}, \qquad \text{(A7)}$$

where $\delta_{\text{in},x}^2(\delta_{\text{in}}^2, p)$ is the initial variance of the qunaught state in the x (p) quadrature before an optical switch. After beam splitter coupling between two qunaught states, the GKP-Bell pair, where each peak has the variance of $\delta_{\text{in},x}^2 + 1 - \eta_{\text{in}}$, is generated. We note that variances of one of the modes of the GKP-Bell pair in the x and p quadratures are equal to those of the qunaught states.

Figure 10 shows the error probability of the $\hat{F}\hat{F}\hat{C}_z$ gate using the Knill-type QEC. Numerical results imply that fault-tolerant quantum computation with the squeezing level 15 and 20 dB will be possible up to loss parameters around 0.5 and 2.0%, respectively, since the error probability of $\hat{F}\hat{F}\hat{C}_z$ required for the fault-tolerant quantum computation is generally assumed to be around 1.0%.

3. Error probability of $\hat{F}\hat{F}\hat{C}_Z$ with the proposed method

To calculate the error probability of the two-mode gate (thus the error threshold) of our proposed method, we consider the nullifiers of the two-sided tree graph. In our proposed setup, we employ the two types of the Bell state, e.g., the Bell state of the squeezed vacuum states (two-mode squeezed states) and that of GKP qubits. These two types of Bell states are used for measurement-based quantum computation (MBQC) and QEC, respectively. Those Bell states are prepared from the two-sided tree graph described in Fig. 7 in the main text, where the two-sided tree graph is prepared from the two-sided tree graph state. The nullifiers for the tree graph state are

$$\hat{\delta}_1 = \hat{p}_1 - \hat{x}_a - \sum_{k\in\mathcal{K}}\hat{x}_k, \quad \hat{\delta}_2 = \hat{p}_2 - \hat{x}_b - \sum_{l\in\mathcal{L}}\hat{x}_l, \qquad \text{(A8)}$$

$$\hat{\delta}_k = \hat{p}_k - \hat{x}_1, \quad \hat{\delta}_l = \hat{p}_l - \hat{x}_2, \qquad \text{(A9)}$$

$$\hat{\delta}_a = \hat{p}_a - \hat{x}_1, \quad \hat{\delta}_b = \hat{p}_b - \hat{x}_2, \qquad \text{(A10)}$$

where the labels 1, 2, k, and l correspond to the modes for the two-sided tree graph in Fig. 7 in the main text, and the labels a and b correspond to the modes used for the Bell measurement to prepare the two-sided tree graph. Although the variances of the nullifiers are zero in the ideal case, for the physical finite squeezing, the nullifiers will be nonzero. After the Bell measurement, the values of the nullifiers that are associated with mode a and b will be increased due to the finite squeezing.

Here we describe the variances for the Bell state of squeezed vacuums and the GKP qubits. For simplicity, we will assume that the two-sided tree graph state is symmetric and the number of the mode n is given by $n = 2N + 2$, where N is the number of the branches on each side. When we consider the teleportation protocol, the amount of the squeezing in the Einstein-Podolsky-Rosen correlation is what determines the noise of the protocol. Similarly, although the variance of the nullifier becomes zero for the ideal state, the variance will always be finite for the actual physical system. For the Bell state of squeezed vacuums used for MBQC, after we disentangle mode k (l) from mode 1 (2), the variance for the mode 1 (2) via the measurement in the x quadrature and the variances of the nullifiers of the resultant two-mode entanglement state have the values as if the state is generated using p-squeezed states whose squeezing level is $(N + 2)\sigma^2$ and the ideal controlled-Z gate. We can easily verify this by looking at the variances of the nullifiers given in Eqs. (8)–(11). For the Bell state of GKP qubits used for the QEC, we disentangle mode k (l) from mode 1 (2), while we select the measurement bases so that a mode of the GKP qubit is successfully prepared in the quantum memory [which we will label as mode i (j)], entangled with mode 1 (2). After the measurements, the width of the peaks of the GKP qubit will become $2\sigma^2$ and $(N + 2)\sigma^2$ for x and p quadratures, respectively. Note that there is additional σ^2 compared to the Bell state of the squeezed vacuum due to the finite squeezing of the GKP qubit.

With the preparations above, we now calculate the error probability of the $\hat{F}\hat{F}\hat{C}_Z$ gate for our proposed scheme. The $\hat{C}_Z$

gate between input modes 1 and 2 transforms the peak width of the GKP state as

$$\tilde{\delta}^2_{x_{\text{in}}1(2)} \mapsto \tilde{\delta}^2_{x_{\text{in}}1(2)}, \tag{A11}$$

$$\tilde{\delta}^2_{p_{\text{in}}1(2)} \mapsto \tilde{\delta}^2_{p_{\text{in}}1(2)} + \tilde{\delta}^2_{x_{\text{in}}2(1)}, \tag{A12}$$

where $\tilde{\delta}^2_{x_{\text{in}}1(2)}$ and $\tilde{\delta}^2_{p_{\text{in}}1(2)}$ are the initial variances of GKP qubits in the x and p quadratures, respectively. Then, after the $\hat{F}$ gate on the input mode 1 (2), additional noise variance $\tilde{\xi}$ from the Bell state of the squeezed vacuum is added to the variance of the the mode 1 (2) in both x and p quadratures, where $\tilde{\xi}$ is given as

$$\tilde{\xi} = (N+1)\sigma^2. \tag{A13}$$

As a consequence, the noise variances for the $\hat{F}\hat{F}\hat{C}_Z$ gate become

$$\tilde{\xi}_x = \tilde{\delta}^2_{p_{\text{in}}1(2)} + \tilde{\delta}^2_{x_{\text{in}}1(2)} + \tilde{\xi}, \tag{A14}$$

$$\tilde{\xi}_p = \tilde{\delta}^2_{x_{\text{in}}1(2)} + \tilde{\xi}. \tag{A15}$$

Then we implement the QEC using the Bell state of the GKP qubits. In the QEC, after the beam splitter coupling between the input mode and one of the Bell state, the variances of the input mode in the x quadrature and that of the Bell state in the p quadrature become $\tilde{\xi}_p + (N+2)\sigma^2$ and $\tilde{\xi}_x + 2\sigma^2$, respectively. This corresponds to a sum of the variances of the data and the ancilla GKP qubits. Thus, the error probability of the QECs can be calculated from the noise variances $\sigma^2_{1(2),x} = \tilde{\xi}_p + (N+2)\sigma^2$ and $\sigma^2_{1(2),p} = \tilde{\xi}_x + 2\sigma^2$, resulting in the graph in Fig. 8.

4. Optical loss with amplifications

In the Heisenberg picture, a loss channel with the efficiency η transforms the quadratures as

$$\hat{x} \to \sqrt{\eta}\hat{x} + \sqrt{1-\eta}\hat{x}_{\text{vac}}, \quad \hat{p} \to \sqrt{\eta}\hat{p} + \sqrt{1-\eta}\hat{p}_{\text{vac}}, \tag{A16}$$

where $\hat{x}_{\text{vac}}$ ($\hat{p}_{\text{vac}}$) is the position (momentum) quadrature of an ancillary vacuum state. This results in the transformation of the variances as

$$\sigma^2_{\text{in},x} \to \eta\sigma^2_{\text{in},x} + \frac{1-\eta}{2}, \tag{A17}$$

$$\sigma^2_{\text{in},p} \to \eta\sigma^2_{\text{in},p} + \frac{1-\eta}{2}, \tag{A18}$$

where $\sigma^2_{\text{in},x}$ ($\sigma^2_{\text{in},p}$) are variances of the initial states before the loss channel.

From Eq. (A16), we observe that the positions of the peaks of the GKP qubits are deamplified by a factor $\sqrt{\eta}$. To recover the codeword of the GKP qubit in both x and p quadratures simultaneously, a phase insensitive amplification with an amplification factor of $1/\sqrt{\eta}$ is used. This amplification transforms the quadratures as

$$\hat{x} \to \sqrt{\frac{1}{\eta}}\hat{x} + \sqrt{\frac{1}{\eta} - 1}\hat{x}_{\text{vac}}, \tag{A19}$$

$$\hat{p} \to \sqrt{\frac{1}{\eta}}\hat{p} + \sqrt{\frac{1}{\eta} - 1}\hat{p}_{\text{vac}}. \tag{A20}$$

Therefore, this amplification transforms the variance of the input state as

$$\sigma^2_{\text{in},x} \to \frac{1}{\eta}\sigma^2_{\text{in},x} + \frac{1-\eta}{2\eta}, \tag{A21}$$

$$\sigma^2_{\text{in},p} \to \frac{1}{\eta}\sigma^2_{\text{in},p} + \frac{1-\eta}{2\eta}. \tag{A22}$$

Now we describe two amplification techniques used in the recovery of the codewords of the GKP qubits. First, we explain the amplification after the loss channel, which we refer to as *postamplification* . In this case, the variance after both loss channel and amplification in both quadratures is

$$\sigma^2_{\text{in},x(p)} \to \sigma^2_{\text{in},x(p)} + \frac{1-\eta}{\eta}, \tag{A23}$$

where σ^2_{in} is the initial variance. We observe that the additional noise $(1-\eta)/\eta$ comes from both the loss channel and the phase insensitive amplification.

Second, we consider the amplification before photon loss, which we refer to as *preamplification*. For this case, the variances are transformed as

$$\sigma^2_{\text{in},x(p)} \to \sigma^2_{\text{in},x(p)} + 1 - \eta. \tag{A24}$$

We observe that preamplification introduces less noise than the postamplification [51]. In our paper, to compare and consider the performance of the conventional scheme using optical switches, we employ the preamplification technique before an optical switch to implement the QEC with GKP qubits.

[1] S. Takeda and A. Furusawa, Toward large-scale fault-tolerant universal photonic quantum computing, APL Photon. **4**, 060902 (2019).

[2] S. Slussarenko and G. J. Pryde, Photonic quantum information processing: A concise review, Appl. Phys. Rev. **6**, 041303 (2019).

[3] N. C. Menicucci, Temporal-mode continuous-variable cluster states using linear optics, Phys. Rev. A **83**, 062314 (2011).

[4] R. Raussendorf and H. J. Briegel, A One-Way Quantum Computer, Phys. Rev. Lett. **86**, 5188 (2001).

[5] N. C. Menicucci, P. van Loock, M. Gu, C. Weedbrook, T. C. Ralph, and M. A. Nielsen, Universal Quantum Computation

with Continuous-Variable Cluster States, Phys. Rev. Lett. **97**, 110501 (2006).

[6] S. Yokoyama, R. Ukai, S. C. Armstrong, C. Sornphiphatphong, T. Kaji, S. Suzuki, J. Yoshikawa, H. Yonezawa, N. C. Menicucci, and A. Furusawa, Ultra-large-scale continuous-variable cluster states multiplexed in the time domain, Nat. Photon. **7**, 982 (2013).

[7] J. Yoshikawa, S. Yokoyama, T. Kaji, C. Sornphiphatphong, Y. Shiozawa, K. Makino, and A. Furusawa, Invited article: Generation of one-million-mode continuous-variable cluster state by unlimited time-domain multiplexing, APL Photon. **1**, 060801 (2016).

[8] W. Asavanant, Y. Shiozawa, S. Yokoyama, B. Charoensombutamon, H. Emura, R. N. Alexander, S. Takeda, J. Yoshikawa, N. C. Menicucci, H. Yonezawa, and A. Furusawa, Generation of time-domain-multiplexed two-dimensional cluster state, Science **366**, 373 (2019).

[9] M. V. Larsen, X. Guo, C. R. Breum, J. S. Neergaard-Nielsen, and U. L. Andersen, Deterministic generation of a two-dimensional cluster state, Science **366**, 369 (2019).

[10] W. Asavanant, B. Charoensombutamon, S. Yokoyama, T. Ebihara, T. Nakamura, R. N. Alexander, M. Endo, J. Yoshikawa, N. C. Menicucci, H. Yonezawa, and A. Furusawa, Time-Domain-Multiplexed Measurement-Based Quantum Operations with 25-MHz Clock Frequency, Phys. Rev. Appl. **16**, 034005 (2021).

[11] M. V. Larsen, X. Guo, C. R. Breum, J. S. Neergaard-Nielsen, and U. L. Andersen, Deterministic multi-mode gates on a scalable photonic quantum computing platform, Nat. Phys. **17**, 1018 (2021).

[12] O. Pfister, Continuous-variable quantum computing in the quantum optical frequency comb, J. Phys. B: At. Mol. Opt. Phys. **53**, 012001 (2020).

[13] R. N. Alexander, P. Wang, N. Sridhar, M. Chen, O. Pfister, and N. C. Menicucci, One-way quantum computing with arbitrarily large time-frequency continuous-variable cluster states from a single optical parametric oscillator, Phys. Rev. A **94**, 032327 (2016).

[14] R. Yang, J. Zhang, S. Zhai, K. Liu, J. Zhang, and J. Gao, Generating multiplexed entanglement frequency comb in a non-degenerate optical parametric amplifier, J. Opt. Soc. Am. B **30**, 314 (2013).

[15] R. Yang, J. Wang, J. Zhang, K. Liu, and J. Gao, Generation of continuous-variable spatial cluster entangled states in optical mode comb, J. Opt. Soc. Am. B **33**, 2424 (2016).

[16] E. Meyer-Scott, C. Silberhorn, and A. Migdall, Single-photon sources: Approaching the ideal through multiplexing, Rev. Sci. Instrum. **91**, 041101 (2020).

[17] J. Carolan, C. Harrold, C. Sparrow, E. Martín-López, N. J. Russell, J. W. Silverstone, P. J. Shadbolt, N. Matsuda, M. Oguma, M. Itoh, G. D. Marshall, M. G. Thompson, J. C. F. Matthews, T. Hashimoto, J. L. O'Brien, and A. Laing, Universal linear optics, Science **349**, 711 (2015).

[18] M. V. Larsen, X. Guo, C. R. Breum, J. S. Neergaard-Nielsen, and U. L. Andersen, Fiber-coupled EPR-state generation using a single temporally multiplexed squeezed light source, npj Quantum Inf. **5**, 46 (2019).

[19] R. N. Alexander, S. Yokoyama, A. Furusawa, and N. C. Menicucci, Universal quantum computation with temporal-mode bilayer square lattices, Phys. Rev. A **97**, 032302 (2018).

[20] S. Takeda and A. Furusawa, Universal Quantum Computing with Measurement-Induced Continuous-Variable Gate Sequence in a Loop-Based Architecture, Phys. Rev. Lett. **119**, 120504 (2017).

[21] M. V. Larsen, C. Chamberland, K. Noh, J. S. Neergaard-Nielsen, and U. L. Andersen, Fault-tolerant continuous-variable measurement-based quantum computation architecture, PRX Quantum **2**, 030325 (2021).

[22] S. Takeda, K. Takase, and A. Furusawa, On-demand photonic entanglement synthesizer, Sci. Adv. **5**, eaaw4530 (2019).

[23] W. Yoshiki and T. Tanabe, All-optical switching using kerr effect in a silica toroid microcavity, Opt. Express **22**, 24332 (2014).

[24] D. Gottesman, A. Kitaev, and J. Preskill, Encoding a qubit in an oscillator, Phys. Rev. A **64**, 012310 (2001).

[25] K. Fukui, A. Tomita, A. Okamoto, and K. Fujii, High-Threshold Fault-Tolerant Quantum Computation with Analog Quantum Error Correction, Phys. Rev. X **8**, 021054 (2018).

[26] K. Fukui, A. Tomita, and A. Okamoto, Analog Quantum Error Correction with Encoding a Qubit into an Oscillator, Phys. Rev. Lett. **119**, 180507 (2017).

[27] N. C. Menicucci, Fault-Tolerant Measurement-Based Quantum Computing with Continuous-Variable Cluster States, Phys. Rev. Lett. **112**, 120504 (2014).

[28] E. Knill, Scalable quantum computing in the presence of large detected-error rates, Phys. Rev. A **71**, 042322 (2005).

[29] B. W. Walshe, L. J. Mensen, B. Q. Baragiola, and N. C. Menicucci, Robust fault tolerance for continuous-variable cluster states with excess antisqueezing, Phys. Rev. A **100**, 010301(R) (2019).

[30] M. V. Larsen, J. S. Neergaard-Nielsen, and U. L. Andersen, Architecture and noise analysis of continuous-variable quantum gates using two-dimensional cluster states, Phys. Rev. A **102**, 042608 (2020).

[31] R. N. Alexander and N. C. Menicucci, Flexible quantum circuits using scalable continuous-variable cluster states, Phys. Rev. A **93**, 062326 (2016).

[32] S. Lloyd and S. L. Braunstein, Quantum Computation over Continuous Variables, Phys. Rev. Lett. **82**, 1784 (1999).

[33] M. Yukawa, R. Ukai, P. van Loock, and A. Furusawa, Experimental generation of four-mode continuous-variable cluster states, Phys. Rev. A **78**, 012301 (2008).

[34] P. van Loock, C. Weedbrook, and M. Gu, Building gaussian cluster states by linear optics, Phys. Rev. A **76**, 032321 (2007).

[35] R. Ukai, J. Yoshikawa, N. Iwata, P. van Loock, and A. Furusawa, Universal linear Bogoliubov transformations through one-way quantum computation, Phys. Rev. A **81**, 032315 (2010).

[36] J. Yoshikawa, K. Makino, S. Kurata, P. van Loock, and A. Furusawa, Creation, Storage, and On-Demand Release of Optical Quantum States with a Negative Wigner Function, Phys. Rev. X **3**, 041028 (2013).

[37] D. Gottesman and I. L. Chuang, Demonstrating the viability of universal quantum computation using teleportation and single-qubit operations, Nature (London) **402**, 390 (1999).

[38] J. Hastrup, M. V. Larsen, J. S. Neergaard-Nielsen, N. C. Menicucci, and U. L. Andersen, Unsuitability of cubic phase gates for non-Clifford operations on Gottesman-Kitaev-Preskill states, Phys. Rev. A **103**, 032409 (2021).

[39] S. Konno, W. Asavanant, K. Fukui, A. Sakaguchi, F. Hanamura, P. Marek, R. Filip, J. Yoshikawa, and A. Furusawa, Non-Clifford gate on optical qubits by nonlinear feedforward, Phys. Rev. Res. **3**, 043026 (2021).

[40] B. W. Walshe, B. Q. Baragiola, R. N. Alexander, and N. C. Menicucci, Continuous-variable gate teleportation and bosonic-code error correction, Phys. Rev. A **102**, 062411 (2020).

[41] B. W. Walshe, R. N. Alexander, N. C. Menicucci, and B. Q. Baragiola, Streamlined quantum computing with macronode cluster states, Phys. Rev. A **104**, 062427 (2021).

[42] K. Suzuki, R. Konoike, S. Suda, H. Matsuura, S. Namiki, H. Kawashima, and K. Ikeda, Low-loss, low-crosstalk, and large-scale optical switch based on silicon photonics, J. Lightwave Technol. **38**, 233 (2020).

[43] H. Vahlbruch, M. Mehmet, K. Danzmann, and R. Schnabel, Detection of 15 dB Squeezed States of Light and their Application for the Absolute Calibration of Photoelectric Quantum Efficiency, Phys. Rev. Lett. **117**, 110801 (2016).

[44] C. Flühmann, T. L. Nguyen, M. Marinelli, V. Negnevitsky, K. Mehta, and J. P. Home, Encoding a qubit in a trapped-ion mechanical oscillator, Nature (London) **566**, 513 (2019).

[45] P. Campagne-Ibarcq, A. Eickbusch, S. Touzard, E. Zalys-Geller, N. E. Frattini, V. V. Sivak, P. Reinhold, S. Puri, S. Shankar, R. J. Schoelkopf, L. Frunzio, M. Mirrahimi, and M. H. Devoret, Quantum error correction of a qubit encoded in grid states of an oscillator, Nature (London) **584**, 368 (2020).

[46] I. Tzitrin, J. E. Bourassa, N. C. Menicucci, and K. K. Sabapathy, Progress towards practical qubit computation using approximate Gottesman-Kitaev-Preskill codes, Phys. Rev. A **101**, 032315 (2020).

[47] K. Fukui, S. Takeda, M. Endo, W. Asavanant, J. Yoshikawa, P. van Loock, and A. Furusawa, Efficient Backcasting Search for Optical Quantum State Synthesis, Phys. Rev. Lett. **128**, 240503 (2022).

[48] K. Fukui, M. Endo, W. Asavanant, A. Sakaguchi, J. Yoshikawa, and A. Furusawa, Generating the Gottesman-Kitaev-Preskill qubit using a cross-Kerr interaction between squeezed light and Fock states in optics, Phys. Rev. A **105**, 022436 (2022).

[49] Y. Hashimoto, T. Toyama, J. Yoshikawa, K. Makino, F. Okamoto, R. Sakakibara, S. Takeda, P. van Loock, and A. Furusawa, All-Optical Storage of Phase-Sensitive Quantum States of Light, Phys. Rev. Lett. **123**, 113603 (2019).

[50] N. C. Menicucci, S. T. Flammia, and P. van Loock, Graphical calculus for Gaussian pure states, Phys. Rev. A **83**, 042335 (2011).

[51] K. Noh, V. V. Albert, and L. Jiang, Quantum capacity bounds of Gaussian thermal loss channels and achievable rates with Gottesman-Kitaev-Preskill codes, IEEE Trans. Inf. Theory **65**, 2563 (2019).